# A Performance Evaluation of a Microchannel Reactor for the Production of Hydrogen from Formic Acid for Electrochemical Energy Applications

*Isabella M. Ndlovu[1], Raymond C. Everson[1], Steven Chiuta[1], Hein W.J.P. Neomagus[1], Henrietta W. Langmi[2], Jianwei Ren[2], Nicolaas Engelbrecht[1] and Dmitri G. Bessarabov[1,\*]*

[1] HySA Infrastructure Centre of Competence, North-West University, Faculty of Engineering, Private Bag X6001, Potchefstroom, 2520, South Africa
[2] HySA Infrastructure Centre of Competence, Materials Science and Manufacturing, Council for Scientific and Industrial Research (CSIR), PO Box 395, Pretoria, 0001, South Africa
[\*]E-mail: Dmitri.Bessarabov@nwu.ac.za

An experimental evaluation of a microchannel reactor was completed to assess the reactor performance for the catalytic decomposition of vaporised formic acid (FA) for $H_2$ production. Initially, X-ray powder diffraction (XRD), elemental mapping using SEM-EDS and BET surface area measurements were done to characterise the commercial $Au/Al_2O_3$ catalyst. The reactor was evaluated using pure (99.99%) and diluted (50/50 vol.%) FA at reactor temperatures of 250–350°C and inlet vapour flow rates of 12–48 mL.min$^{-1}$. Satisfactory reactor performance was demonstrated at 350°C as near-equilibrium FA conversion (>98%) was obtained for all flow rates investigated. The best operating point was identified as 350°C and 48 mL.min$^{-1}$ (pure FA feed) with a $H_2$ yield of 68.7%. At these conditions the reactor performed well in comparison to conventional systems, achieving a $H_2$ production rate of 11.8 NL.g$_{cat}^{-1}$.h$^{-1}$. This paper therefore highlights important considerations for ongoing design and development of microchannel reactors for the decomposition of FA for $H_2$ production.

**Keywords:** Formic acid decomposition; hydrogen production; microchannel reactor; fuel cell application; $Au/Al_2O_3$ catalyst
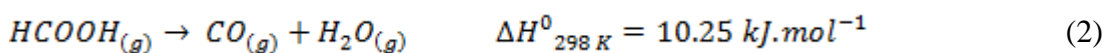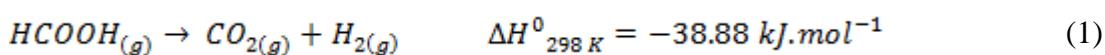
| NOMENCLATURE | | ABBREVIATIONS | |
|---|---|---|---|
| H | Height, m | BASF | Badische Anilin- und Soda-Fabrik |
| $\Delta H_r$ | Enthalpy of reaction, J.mol$^{-1}$ | BET | Brunauer-Emmett-Teller |
| L | Length, m | d.b | Dry basis |
| $LHV_{H2}$ | Hydrogen lower heating value, | DST | Department of Science and Technology |

| $M_{H2}$ | Hydrogen mass flow, $kg.s^{-1}$ | EDS | Energy–Dispersive X-ray Spectroscopy |
|---|---|---|---|
| $P_{H2}$ | Hydrogen thermal wattage, W | FA | Formic acid |
| $S_{H2}$ | Hydrogen selectivity | GC | Gas chromatograph |
| W | Width, m | LPG | Liquefied petroleum gas |
| $X_{FA}$ | Formic acid conversion, % | LTHFC | Low temperature hydrogen fuel cell |
| $Y_{H2}$ | Hydrogen yield, % | SEM | Scanning Electron Microscopy |
| $yi$ | Mole fraction of component i | SOFC | Solid oxide fuel cell |
| *SUBSCRIPTS & SUPERSCRIPTS* | | vol.% | Volume percent |
| a | Absolute | WGS | Water-gas-shift reaction |
| cat | Catalyst | wt.% | Weight percent |
| g | Gas | XRD | X-ray powder diffraction |
| r | Reaction | | |

# 1. INTRODUCTION

As the global energy demand increases, hydrogen ($H_2$) is considered to be a versatile energy carrier due to its high gravimetric energy density (142 MJ/kg) and carbon-free structure [1]. As a result, distributed power generation through hydrogen & fuel cell-based technologies is an attractive prospect considering near-zero emissions and uninterrupted power supply. The storage and transportation of compressed hydrogen however poses numerous safety risks due to its high flammability and quick diffusion rate into the atmosphere [2]. Hydrogen's low volumetric energy density also requires large storage vessels, increasing equipment cost [3,4].

Formic acid (FA) has recently gained attention as a hydrogen dense energy carrier (53.5 kg $H_2/m^3$) as it appears in the liquid state at standard conditions [5]. Transportation and storage infrastructure is therefore simplified as vessels are not pressurised [6–8]. In 2014, BASF produced approximately 255,000 metric tons of FA in Germany and China alone [9]. Global production capacity therefore facilitates large-scale FA-based reforming technologies. Moreover, FA can also be produced from the hydrogenation of carbon dioxide ($CO_2$) resulting in a carbon neutral process [10–13]. Another advantage lies in the fact that the production of $H_2$ from FA is achieved at lower temperatures compared to the reforming of other liquid carriers such as methanol [10]. Studies in direct fuel cell applications have also reported direct FA fuel cells are preferred to the commonly used direct methanol fuel cells [14–17]. Despite the attractive characteristics of FA, its decomposition was historically only studied as a model reaction for catalyst selection [18–21].Various metal catalyst surfaces proved active for FA decomposition following the dehydrogenation (Eq.(1)) and dehydration (Eq.(2)) reaction pathways [22].

$$HCOOH_{(g)} \rightarrow CO_{2(g)} + H_{2(g)} \qquad \Delta H^0_{298\,K} = -38.88 \; kJ.mol^{-1} \qquad (1)$$

$$HCOOH_{(g)} \rightarrow CO_{(g)} + H_2O_{(g)} \qquad \Delta H^0_{298\,K} = 10.25 \; kJ.mol^{-1} \qquad (2)$$

It is however important to suppress the dehydration pathway to avoid fuel cell catalyst poisoning due to carbon monoxide (CO) presence. As a result, active and selective catalyst development has been the main theme in recent studies related to FA decomposition for $H_2$ production. Noticeable advances have been made in the decomposition of FA with the use of homogeneous catalysts of ruthenium (Ru) and rhodium (Rh) [1,23–29]. Recently, heterogeneous catalysts of gold (Au) and platinum group metals (Pt, Rh, Ir) are preferred as catalyst recuperation and recycling is simplified [30–33]. Other complex bimetallic and tri-metallic catalysts of silver (Ag), palladium (Pd) and Au were also developed to improve the activity of equivalent monometallic catalyst [34–40].

Despite numerous studies on catalyst development for FA decomposition, few studies focussed on the design and development of novel reactor technologies for improved heat and mass transfer. The catalytic decomposition of FA has been carried out in laboratory-scale fixed-bed [30,31,41], packed-bed [33,42] and stirred tank reactors [1,35]. Large temperature gradients often exist within conventional flow reactors, reducing overall reactor performance [38]. Moreover, these reactors lack compactness required for turn-key applications. As a result, a micro tubular reactor (0.5 mm ID) with wall-coated catalyst was evaluated for FA decomposition [43]. It was reported that the reactor showed process intensifying properties and good performance. Evidently, compact reactors provide increased volumetric throughput and better thermal efficiencies. Microchannel reactors are often considered as process intensifying [44,45] and have large surface to volume ratios, shortening diffusion lengths and improving heat and mass transfer effects [46–49].

Thus far, microchannel reactors have been identified in numerous studies as a reactor technology that inherently satisfies the strict requirements (high conversion and increased throughput) for portable and distributed $H_2$ generation [4,50–57]. Currently, there are no experimental work reporting on the use of microchannel reactors for FA decomposition. In this paper, the advantages of an active heterogeneous catalyst ($Au/Al_2O_3$) for FA decomposition were combined with that of a microchannel reactor for $H_2$ production. The effect of varying operating conditions (i.e. temperature, inlet flow rate and pure/diluted FA feed) on reactor performance was determined.

## 2. METHODOLOGY

This section describes the design, development and operation of the microchannel reactor for FA decomposition.

### 2.1 Experimental apparatus

A microchannel reactor (German grade SS314) was constructed in collaboration with Fraunhofer-ICT-IMM (Mainz, Germany). A similar reactor design was used in previous work by our research group and showed good performance for $NH_3$ decomposition [57,58] and $CO_2$ methanation [59], respectively. The reactor design consisted of eighty microchannels (W = 450 µm, H = 150 µm and L = 50 mm) engraved according to a wet chemical etching method described elsewhere [60]. Finally, a commercial 1.15 wt.% $Au/Al_2O_3$ catalyst (79-0160™, Mintek, South Africa) was washcoated onto the fabricated reactor plate [56,60].

A process flow diagram of the experimental apparatus is illustrated in Fig. 1. A syringe pump (NE-1000 series) was used to control the flow rate of liquid FA to an evaporator. The evaporator was heated by a heating cartridge (HI-TECH elements) and the temperature controlled with integrated K-type thermocouples. The FA vapour subsequently flowed to the microchannel reactor. The reactor was heated to predetermined temperatures by two heating cartridges (Watlow FIREROD®, 300W each), and two additional K-type thermocouples were used to measure the reactor wall temperature on opposite ends of the reactor. Product fractions were analysed using an online GC (SRI 8610C).
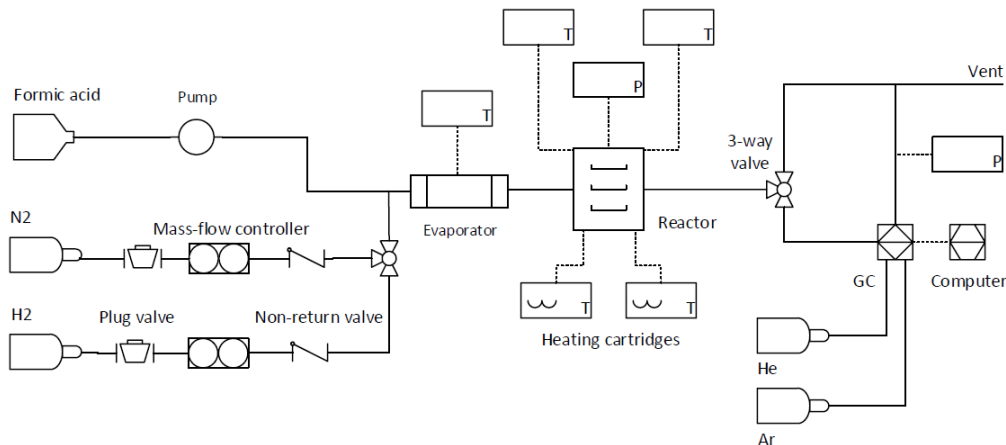


**Figure 1.** Process flow diagram for the production of $H_2$ from formic acid.

## 2.2 Catalyst characterisation

### 2.2.1 X-ray Powder Diffraction and Scanning Electron Microscopy
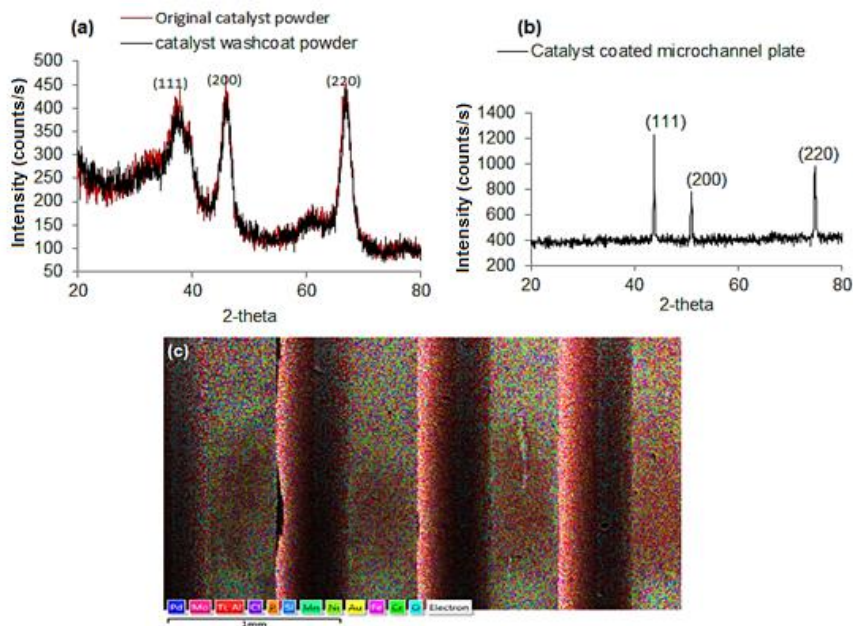


**Figure 2.** (a) XRD pattern of the original catalyst and washcoat catalyst powder, (b) XRD pattern of the catalyst coated microchannel plate and (c) EDS map of the catalyst coated microchannel plate.

X-ray powder diffraction (XRD) patterns were obtained from a PANalytical X'Pert Pro powder diffractometer with Pixcel detector using Ni-filtered Cu-K$_\alpha$ radiation (0.154 nm) and scanning rate of 0.1°/s. There were no obvious differences in the XRD patterns (Fig. 2a) of the original catalyst and washcoat catalyst powder. Both patterns exhibited three low intensity broad diffraction peaks typical of nano-sized crystallites, assigned to the (111), (200) and (220) reflections of the Au catalyst. The final washcoated catalyst (Fig. 2b) however showed distinct (111), (200) and (220) reflections, attributed to the Au catalyst, with a shift of peak positions to higher 2-theta values suggesting a decrease in lattice parameter after the washcoating, drying and calcination procedure employed. Elemental mapping was carried out using an Auriga Cobra Focused-Ion Beam Scanning Electron Microscope (FIB-SEM) equipped with Energy-Dispersive X-ray Spectroscopy (EDS). The SEM-EDS mapping of the catalyst coated plate (Fig. 2c) showed strong characteristic peaks of the stainless steel material used to construct the reactor plates. The presence of some elements in stainless steel (Fe, Cr, Ni, Mn, Mo, Si and P) were detected. The catalytic effects of these elements on FA decomposition are however unknown. The EDS pattern also showed the presence of Cl, attributed to the use of an iron chloride solution during the chemical etching process.

### 2.2.2 BET surface area measurement

Catalyst surface area measurements were carried out using a Micromeritics ASAP 2020 HD analyser and the BET surface areas were obtained from the $N_2$ isotherms. The BET surface area of the washcoated catalyst was found to be higher (130 m².g$^{-1}$) than that of the original catalyst powder (78 m².g$^{-1}$). The increase in surface area is attributed to the specific washcoating and calcination process used, which may have increased the catalyst porosity and particle dispersion across the microchannels [56].

### 2.3 Experimental procedure

Prior to experiments, the catalyst was reduced in $H_2$ (50 mL.min$^{-1}$) at 400°C for 2 h [30]. Daily reactor start-up and shutdown procedures were initiated under $N_2$ flow (50 mL.min$^{-1}$) to prevent catalyst thermal degradation. Two sets of experiments were performed comprising of pure FA (99.99%) and a FA/$H_2O$ mixture (50/50 vol.%) as feed to the evaporator. The microchannel reactor was evaluated by investigating the effect of reactor temperature (250–350°C) and vapour inlet flow rate (12–48 mL.min$^{-1}$) at atmospheric pressure (0.88 bar). Importantly, all experiments were conducted in the gas phase. The repeatability of data was also investigated and found to be reproducible within a relative error of ±4%.

## 3. RESULTS AND DISCUSSION

The microchannel reactor's performance was evaluated on parameters defined as FA conversion (Eq. 3), $H_2$ selectivity (Eq. 4), $H_2$ yield (Eq. 5) and equivalent $H_2$ power output (Eq. 6). These parameters satisfy the conservation of mass among all product species. Equilibrium data (Fig.

3–4) was also obtained by the method of Gibbs free energy minimisation at discrete temperature conditions considering both the dehydration and dehydrogenation reactions.

$$X_{FA} = \frac{y_{CO_2} + y_{CO}}{y_{FA} + y_{CO_2} + y_{CO}} \times 100\% \tag{3}$$

$$S_{H_2} = \frac{y_{CO_2}}{y_{CO_2} + y_{CO}} \tag{4}$$

$$Y_{H_2} = S_{H_2} \times X_{FA} \tag{5}$$

$$P_{H_2} = M_{H_2} \times LHV_{H_2} \tag{6}$$

### 3.1 Effect of reactor temperature and inlet flow rate

Throughout the experimental investigation of the microchannel reactor, the commercial 1.15 wt.% $Au/Al_2O_3$ catalyst proved active for the decomposition of FA to produce $H_2$. As reactor temperature increased, higher decomposition rates of FA was obtained (Fig. 3). Ultimately, equilibrium product formation was obtained at 350°C as the outlet $H_2$ fraction (0.415) closely corresponded to the equilibrium value (0.422) on a dry basis.
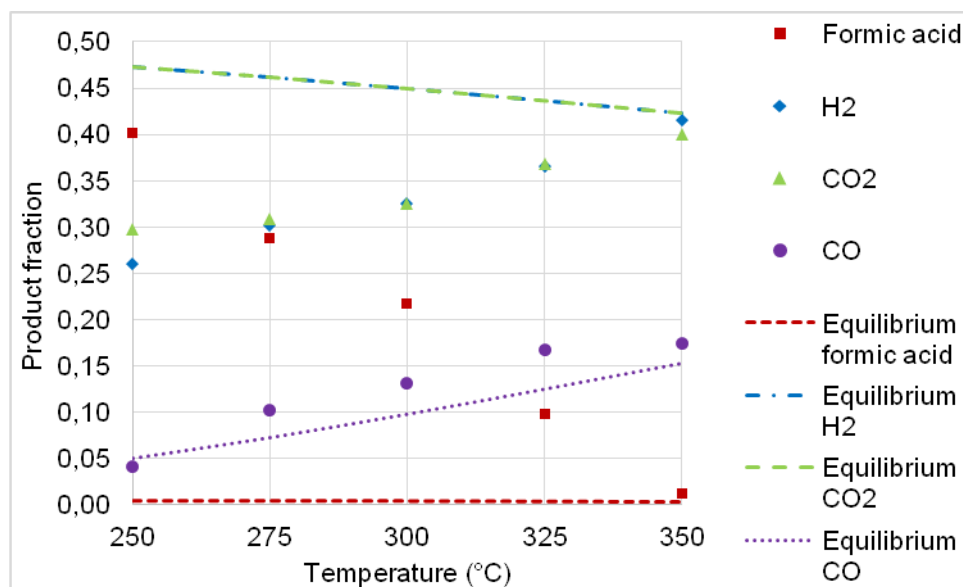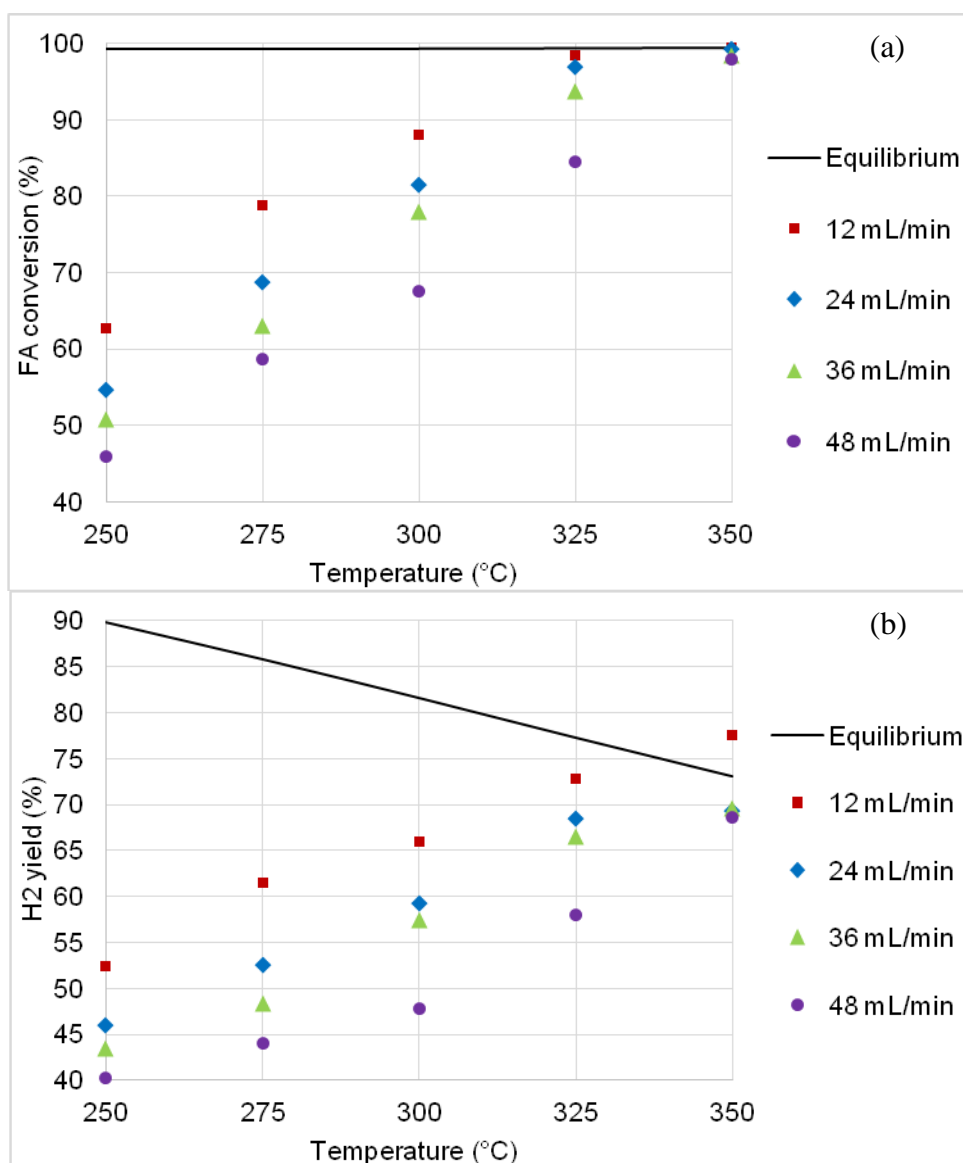


**Figure 3.** Effect of reactor temperature on experimental product composition (d.b) for 48 mL.min^{-1}.

In general, FA conversion improved with increasing reactor temperature for all flow conditions (Fig. 4a). As a result, for the 12 and 24 mL.min^{-1} flow conditions near-equilibrium conversion (>98%) was achieved at a reactor temperature as low as 325°C. The highest FA conversion (~100%) was achieved for the lowest flow condition (12 mL.min^{-1}) at 350°C. Unfavorable FA conversions (below 90%) were observed at low temperature (250–300°C) for all flow rates investigated. Also, in the 250–325°C temperature range, increased flow rate had a detrimental effect on FA conversion as shorter contact times between reactants and the catalyst surface was obtained. However, at 350°C

increased flow rates (36 and 48 mL.min^{-1}) achieved near-equilibrium conversion, as was observed for the low flow conditions at 325°C.

Hydrogen selectivity was found to range between 0.69 and 0.88 at the studied conditions, ascertaining the dehydrogenation reaction (Eq. 1) as the dominant reaction. Overall, the $H_2$ selectivity decreased with temperature, attributed to the exothermic nature of the dehydrogenation reaction. Nevertheless, the corresponding $H_2$ yield increased with increasing reactor temperature, as observed for FA conversion (Fig. 4b). Should future experiments be conducted at temperatures above 350°C to facilitate even higher flow rates, lower $H_2$ selectivity and yield would be expected as the endothermic dehydration reaction (Eq. 2) will be favored. Although the highest $H_2$ yield (77.6%) was obtained for the lowest flow rate (12 mL.min^{-1}) at 350°C, it is recommended that a high flow condition (48 mL.min^{-1}) is considered to maximise $H_2$ production. The corresponding $H_2$ yield at this condition is 68.7%.



**Figure 4.** Effect of reactor temperature on (a) FA conversion and (b) $H_2$ yield for 12–48 mL.min^{-1}.

### 3.2 Effect of diluted FA feed

A diluted feed of FA in $H_2O$ (50/50 vol.%) was decomposed aimed at improving $H_2$ selectivity and yield. Carbon monoxide mole fractions (d.b) decreased from 4–17% for the pure FA feed to 2–7% for the diluted FA feed at 48 mL.min$^{-1}$. Accordingly, the corresponding selectivity increased from a range of 0.69–0.88 to 0.81–0.91 across the range of temperatures investigated (Fig. 5a). At 350°C, a significant increase in the $H_2$ yield was noticed (81.0%) compared to the pure feed of FA (68.7%) (Fig. 5b). These results are in accordance with previous literature studies on the effect of added $H_2O$ on the selectivity of Au catalysts [30,33]. Generally, the presence of $H_2O$ in the feed inhibits the dehydration reaction to an extent and promotes the water-gas-shift (WGS) reaction (Eq. 7) [61-63].

$$H_2O_{(g)} + CO_{(g)} \leftrightarrow CO_{2(g)} + H_{2(g)} \qquad \Delta H^0_{298\,K} = -41.1 \; kJ.mol^{-1} \qquad (7)$$
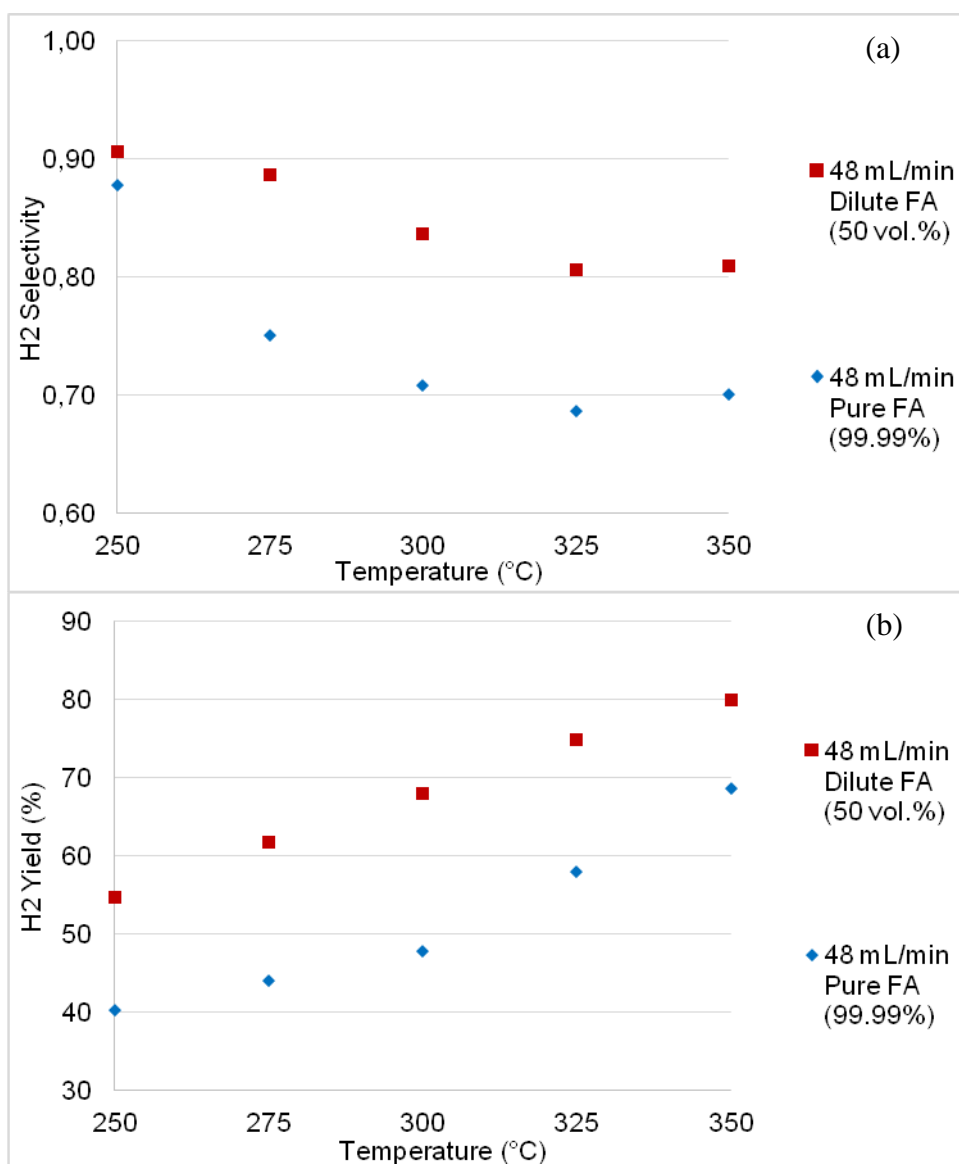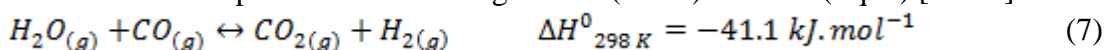


**Figure 5.** Effect of diluted FA feed (50 vol.%) on (a) $H_2$ selectivity and (b) $H_2$ yield for 250–350°C and total inlet flow rate of 48 mL.min$^{-1}$.

*3.3 Recommended operating conditions*

The microchannel reactor provided good performance and catalyst activity at all temperatures (250–350°C) investigated. For a pure feed of FA the 350°C temperature condition achieved the best performance at the lowest flow rate (12 mL.min$^{-1}$) investigated. The highest flow rate (48 mL.min$^{-1}$) however is recommended as $H_2$ production (11.8 NL.g$_{cat}^{-1}$.h$^{-1}$) was maximised with insignificant effect on FA conversion. Yet, throughout the range of operating parameters considered, undesired CO mole fractions (4–17%) were observed. Additional CO clean-up steps (i.e. WGS and preferential oxidation or $H_2$ selective membranes) is therefore recommended for applications related to $H_2$ production for fuel cell power generation. These methods may be used to purify $H_2$ with CO concentrations below 100 ppm required for fuel cell catalyst longevity [34,45,60]. Electrochemical energy applications, such as low temperature hydrogen fuel cells (LTHFC), require pure hydrogen as a fuel. For example, the hydrogen quality for fuel cell applications in transportation in road vehicles is given as 99.97%; it is expressed as the hydrogen fuel index. The fuel specifications are not process or feed stock specific [64]. The described method for hydrogen production in this article still needs additional development to increase hydrogen purity, or development of efficient hydrogen cleanup methods. However, the described technique for hydrogen production may be utilized by several sectors where high- and medium-temperature fuel cells are used. For example, solid oxide fuel cells (SOFC) can be operated on reformed hydrogen or using natural gas or LPG. In the case of electrochemical energy generating systems based on SOFC, the requirements to hydrogen purity is not as strict as for LTHFC. Moreover, endothermic hydrogen generation from formic acid could be integrated and optimized with exothermic conversion of the products of formic acid decomposition in SOFCs. In general, one of the advantages of hydrogen production from formic acid is the ability to generate hydrogen on-demand and on-site, removing the need for hydrogen storage and transport. Key operating parameters are summarised in Table 1.

**Table 1.** Recommended operating conditions for $H_2$ production.

| Parameter | Specification/Value | |
|---|---|---|
| Catalyst | 1.15 wt.% Au/Al$_2$O$_3$ (79-0160™, Mintek, South Africa) | |
| Feed | High purity formic acid (99.99%) | |
| Reactor temperature | 350°C | |
| Reactor pressure | Atmospheric (0.88 bar$_a$) | |
| FA flowrate (vapour) | 48 mL.min$^{-1}$ (17.1 NL.g$_{cat}^{-1}$.h$^{-1}$) | |
| FA conversion | 98% | |
| $H_2$ yield | 68.7% | |
| $H_2$ production rate | 11.8 NL.g$_{cat}^{-1}$.h$^{-1}$ | |
| Product mole fraction (d.b) | FA | 0.012 |
| | $H_2$ | 0.415 |
| | $CO_2$ | 0.399 |
| | CO | 0.174 |

*3.4 Performance comparison with other FA decomposition reactors*

The performance achieved by the microchannel reactor was further compared to that obtained by other reactors in literature for FA decomposition (Table 2). However, unlike previous studies on conventional reactors, this paper investigated FA decomposition in a microchannel reactor. Furthermore, catalyst selection has been the sole purpose in previous studies and as such, parameters critical to reactor performance was rarely reported. For instance, the reactor volume was only reported in [43] while $H_2$ production rates were hardly ever stated. Hydrogen production rates reported in Table 2 were therefore calculated based on reported inlet flowrates, conversions and selectivity values. Finally the thermal power of $H_2$ produced was calculated based on Eq. (6).

Overall, the microchannel reactor reported in this paper performed well in comparison to conventional reactors including fixed-bed [30,31], packed-bed [33] and micro-tubular reactors [43]. More importantly, the reactor achieved conversions close to equilibrium at $350^{\circ}$C, maximizing $H_2$ production rate and thermal wattage. Although similar conversions (>98%) were achieved by other reactors at even lower operating temperatures, the reactor in this paper decomposed highly concentrated FA (99.99%) at a higher throughput (17.1 NL.$g_{cat}^{-1}$.$h^{-1}$). On the other hand, the microchannel reactor resulted in a lower $H_2$ selectivity in comparison to the other reactors. The lower selectivity can be attributed to the differences in catalyst type, catalyst pre-treatment methods as well as metal loading. The implementation of $H_2$ purification technologies is an easy workaround for impurities on supply streams to fuel cells and recommended as an outcome of this work. All results considered, this high throughput microchannel reactor performed well to warranty consideration as a $H_2$ production technology from FA decomposition.

**Table 2.** Comparison of reactor performance for $H_2$ production from FA decomposition

| Reactor Type | Catalyst type | Catalyst weight (g) | Reactor temperature ($^{o}$C) | FA feed | FA flow rate (NL.$g_{cat}^{-1}$.$h^{-1}$) | FA Conversion (%) | $H_2$ Selectivity | $H_2$ yield (%) | $H_2$ production rate (NL.$g_{cat}^{-1}$.$h^{-1}$) | Thermal power of $H_2$ produced (W) |
|---|---|---|---|---|---|---|---|---|---|---|
| *Microchannel | 1.15 wt.% Au /Al$_2$O$_3$ | 0.092 | 350 | 99.99 vol % HCOOH | 17.13 | 97.94 | 0.70 | 68.66 | 11.75 | 2.98 |
| *Microchannel | 1.15 wt.% Au /Al$_2$O$_3$ | 0.092 | 350 | 50 vol % HCOOH/H$_2$O | 8.6 | 98.91 | 0.81 | 80.05 | 6.86 | 1.74 |
| Fixed-bed [30] | 1 wt.% Au /SiO$_2$ | 0.3 | 350 | 7 vol % HCOOH/Ar | 0.56 | 100.00 | 0.95 | 95.00 | 0.53 | 0.44 |
| Fixed-bed [30] | 1 wt.% Au /SiO$_2$ | 0.3 | 250 | 7 vol % HCOOH/Ar | 0.56 | 100.00 | 0.97 | 97.00 | 0.54 | 0.45 |
| Fixed-bed [30] | 1 wt.% Au /Al$_2$O$_3$ | 0.3 | 350 | 7 vol % HCOOH/Ar | 0.56 | 100.00 | 0.11 | 11.00 | 0.06 | 0.05 |
| Fixed-bed [31] | Ir/Cabon Norit | 0.3 | 350 | 6 vol % HCOOH/Ar | 0.48 | 100.00 | 0.93 | 93.00 | 0.45 | 0.37 |
| Fixed-bed [31] | Ir/Cabon Norit | 0.3 | 200 | 6 vol % HCOOH/Ar | 0.48 | 100.00 | 0.98 | 98.30 | 0.47 | 0.39 |
| Packed-bed [33] | 0.8 wt.% Au/Cabon | 0.085 | 317 | 2.4 vol% HCOOH/He | 0.86 | 95.00 | 0.91 | 86.45 | 0.75 | 0.17 |
| Packed-bed [33] | 1 % Pd/Cabon | 0.06 | 127 | 2.4 vol% HCOOH/He | 1.22 | 100.00 | 0.98 | 98.00 | 1.20 | 0.20 |
| Micro-tubular [43] | PdO | 0.0673 | 300 | 0.15 M HCOOH/H$_2$O | 0.01 | 99.20 | 0.99 | 98.41 | 6.44 | 1.19 |

*Results of this work

## 4. CONCLUSIONS

A microchannel reactor was successfully developed and demonstrated for the decomposition of vaporised FA for the production of $H_2$ at different reactor temperatures (250–350°C) and inlet flow rates (12–48 mL.min$^{-1}$). The reactor performed well at the highest temperature considered (350°C), achieving near-equilibrium FA conversion (>98%) for all flow rates investigated. In addition to reactor operation at 350°C, the recommended flow rate is 48 mL.min$^{-1}$ to maximise $H_2$ production. At the recommended operating point the reactor showed a $H_2$ yield of 68.7%. Additional experiments carried out with a diluted feed of FA in $H_2O$ (50/50 vol.%) resulted in increased selectivity towards the dehydrogenation reaction. At these conditions, a $H_2$ yield of 81.0% was obtained. Although good FA conversion was demonstrated, it is recommended that additional CO clean-up techniques be implemented for $H_2$ use in fuel cell applications. Specifically, if the focus of FA decomposition is to maximise $H_2$ production, the implementation of WGS reactors for CO clean-up is an attractive prospect as the WGS reaction produces additional $H_2$. At this stage we envisage that the described technology could be used for niche, small-scale energy applications using SOFC and phosphoric acid medium temperature fuel cells, but can be easily scaled up. Overall, this investigation provided valuable insight into microchannel reactor technology for FA decomposition and can be used as reference for future studies related to the design and development of process intensifying reactors for $H_2$ production.

## References

1. A. Boddien, F. Gärtner, M. Nielsen, S. Losse and H. Junge, *Compr. Inorg. Chem. II,* 9 (2013) 587.
2. R. Lan, J.T.S. Irvine and S. Tao, *Int. J. Hydrogen Energy,* 37 (2012) 1482.
3. C. Zamfirescu and I. Dincer, *J. Power Sources,* 185 (2008) 459.
4. S. Chiuta, R.C. Everson, H.W.J.P. Neomagus, L.A. Le Grange and D.G. Bessarabov, *Int. J. Hydrogen Energy*, 39 (2014) 11390.
5. J. Eppinger and K-W Huang, *ACS Energy Lett.,* 2 (2017) 188.
6. L. Jia, D.A. Bulushev, S. Beloshapkin and J.H.H. Ross, *Appl. Catal. B Environ.,* 160–161 (2014) 35.
7. Q. Zhu, N. Tsumori and Q. Xu, *Chem. Sci.,* 5 (2014) 195.
8. X. Zhou, Y. Huang, C. Liu, J. Liao, T. Lu and W. Xing, *ChemSusChem,* 3 (2010) 1379.
9. BASF Report 2014: Economic, environmental and social performance, 2014, https://www.basf.com/documents/corp/en/about-us/publications/reports/2015/BASF_Report_2014.pdf [accessed on 30.05.17]
10. B. Loges, A. Boddien, F. Gärtner, H. Junge and M. Beller, *Top. Catal.,* 53 (2010) 902.

11. H. Jeon and Y. Chung, *Appl. Catal. B Environ.,* 210 (2017) 212.
12. W. Leitner, *Angew. Chemie Int.*, 107 (1995) 2391.
13. P. Jessop, F. Joo and C. Tai, *Coord. Chem. Rev.*, 248 (2004) 2425.
14. W. Cai, L. Liang, Y. Zhang, W. Xing and C. Liu, *Int. J. Hydrogen Energy,* 38 (2013) 212.
15. W. Cai, L. Yan, C. Li, L. Liang, W. Xing and C. Liu, C, Int. J. Hydrogen Energy, 37 (2012)
a. 3425.
16. S.M. Baik, J. Kim, J. Han and Y. Kwon, *Int. J. Hydrogen Energy*, 36 (2011) 12583.
17. A. Moreno-Zuria, A. Dector, F. M. Cuevas-Muniz, J.P. Esquivel, N. Sabate, J. Ledesma-Garcia, L.G. Arriaga and A.U. Chavez-Ramirez, *J. Power Sources*, 269 (2014) 783.
18. K. Fukuda, T. Onishi and K. Tamaru, *Bull. Chem. Soc. Jpn.,* 42 (1969) 1192.
19. K. Tamaru, *Trans. Faraday Soc.,* 55 (1959) 824.
20. E. Iglesia and M. Boudart, *J. Catal.,* 81 (1983) 214.
21. Y. Noto, K. Fukuda, T. Oniski and K. Tamaru, *Trans. Faraday Soc.,* 63 (1967) 3081.
22. P. Mars, J.J.F. Scholten and P. Zwietering, *Adv. Catal.,* 14 (1963) 35.
23. H. Junge, A. Boddien, F. Capitta, B. Loges, J.R. Noyes, S. Gladiali and M. Beller, *Tetrahedron Lett.,* 50 (2009) 1603.
24. C. Felley, P.J. Dyson and G. Laurenczy, *Angew. Chemie Int.,* 47 (2008) 3966.
25. Y. Himeda, *Green Chem.,* 11 (2009) 2018.
26. A. Boddien, B. Loges, F. Gärtner, C. Torborg, K. Fumino, H. Junge, R. Ludwig and M. Beller, *J. Am. Chem. Soc.,* 132 (2010) 8924.
27. A. Boddien, D. Mellmann, F. Gärtner, R. Jackstell, H. Junge, P.J. Dyson, G. Laurenczy, R. Ludwig and M. Beller, *Science,* 333 (2011) 1733.
28. A. Boddien, F. Gärtner, R. Jackstell, H. Junge, A. Spannenberg, W. Baumann, R. Ludwig and M. Beller, *Angew. Chem. Int.,* 49 (2010) 8993.
29. C. Fellay, N. Yan, P.J. Dyson and G. Laurenczy, *Chem. - A Eur. J.,* 15 (2009) 3752.
30. A. Gazsi, T. Bánsági and F. Solymosi, *J. Phys. Chem. C,* 115 (2011) 15459.
31. F. Solymosi, Á. Koós, N. Liliom and I. Ugrai, *J. Catal.,* 279 (2011) 213.
32. M. Ojeda and E. Iglesia, *Angew. Chemie Int.,* 48 (2009) 4800.
33. D.A. Bulushev, S. Beloshapkin and J.R.H. Ross, *Catal. Today,* 154 (2010) 7.
34. X. Zhou, Y. Huang, W. Xing, C. Liu, J. Liao and T. Lu, *Chem. Commun.,* 30 (2008) 3540.
35. Z.L. Wang, Y. Ping, J.M. Yan, H.L. Wang and Q. Jiang, *Int. J. Hydrogen Energy,* 39 (2014) 4850.
36. S. Zhang, Ö. Metin, D. Su and S. Sun, *Angew. Chemie Int.,* 52 (2013) 3681.
37. K. Tedsree, C.W.A. Chan, S. Jones, Q. Cuan, W.K. Li, X.Q. Gong and S.C.E. Tsang, *Science,* 332 (2011) 224.
38. J. Liu, L. Cao, Y. Xia, W. Huang and Z. Li, *Int. J. Electrochem. Sci.,* 8 (2013) 9435.
39. X. Gu, Z.H. Lu, H.L. Jiang, T. Akita and Q. Xu, *J. Am. Chem. Soc.,* 133 (2011) 11822.
40. Y. Qin, J. Wang, F. Meng, L. Wang and X. Zhang, *Chem. Commun.,* 49 (2013) 10028.
41. Á Koós and F. Solymosi, *Catal. Lett.,* 138 (2010) 23.
42. J.R. Hyde and M. Poliakoff, *Chem. Commun.,* 13 (2004) 1482.
43. R. Javaid, S. Kawasaki, R. Ookawara, K. Sato, M. Nishioka, A. Suzuki and T.M. Suzuki, *J. Chem. Eng. Japan,* 46 (2013) 751.
44. V.R. Regatte and N.S. Kaisare, *Chem. Eng. J.,* 215–216 (2013) 876.
45. J.D. Holladay, Y. Wang and E. Jones, *Chem. Rev.,* 104 (2004) 4767.
46. D. Atkinson and J. McDaniel, *PTQ,* Q2 (2010) 95.
47. J.J. Lerou, A.L. Tonkovich, L. Silva, S. Perry and J. McDaniel, *Chem. Eng. Sci.,* 65 (2010) 380.
48. S. LeViness, P. Schubert, J. McDaniel and T. Dritz, Velocys Fischer-Tropsch Technology. Economical smaller scale GTL enabled by microchannel reactor technology and superactive catalyst, *Syngas Conv.*, Cape Town, South Africa, 2012.
49. G. Kolb and V. Hessel, *Chem. Eng. J.,* 98 (2004) 1.
50. Y. Men, G. Kolb, R. Zapf, V. Hessel and H. Löwe, *Process Saf. Environ. Prot.,* 85 (2007) 413.

51. N.R. Peela, A. Mubayi and D. Kunzru, *Chem. Eng. J.,* 167 (2011) 578.
52. I. Aartun, B. Silberova, H. Venvik, P. Pfeifer, O. Görke, K. Schubert and A. Holmen, *Catal. Today,* 105 (2005) 469.
53. V. Paunovic, J.C. Schouten and T.A. Nijhuis, *Catal. Today,* 248 (2015) 160.
54. M.F. Neira D'Angelo, V. Ordomsky, J. Van Der Schaaf, J.C. Schouten and T.A. Nijhuis, *Int. J. Hydrogen Energy,* 39 (2014) 18069.
55. M. DeSouza, S.H.B. Faria, G.M. Zanini and F.F. Moraes, *Chem. Eng. Trans.,* 32 (2013) 835.
56. R. Zapf, C. Becker-Willinger, K. Berresheim, H. Bolz, H. Gnaser, V. Hessel, G. Kolb, P. Lob, A.K. Pannwitt and A. Ziogas, *Chem. Eng. Res. Des.,* 81 (2003) 721.
57. S. Chiuta, R.C. Everson, H.W.J.P. Neomagus and D.G. Bessarabov, *Int. J. Hydrogen Energy,* 40 (2015) 2921.
58. S. Chiuta, R.C. Everson, H.W.J.P. Neomagus and D.G. Bessarabov, *Int. J. Hydrogen Energy,* 39 (2014) 7225.
59. N. Engelbrecht, S. Chiuta, R.C. Everson, H.W.J.P. Neomagus and D.G. Bessarabov, *Chem. Eng. J.,* 313 (2017) 847.
60. M. O'Connell, G. Kolb, K.P. Schelhaas, M. Wichert, D. Tiemann, H. Pennemann and R. Zapf, *Chem. Eng. Res. Des.,* 90 (2012) 11.
61. P.G. Blake, H.H. Davies and G.E. Jackson, *J. Chem. Soc. B*, (1971) 1923.
62. P.G. Blake and C. Hinshelwood, *Proc. Roy. Soc. A*, 255 (1960) 444.
63. J. Yu and P.E. Savage, *Ind. Eng. Chem. Res.*, 37 (1998) 2.
64. ISO, 2012. Hydrogen fuel – Product specification – Part 2: Proton exchange membrane (PEM) fuel cell applications for road vehicles. International Organization for Standardization (ISO), ISO 14687: 2012. First edition.